THE JOURNAL OF PHYSICAL CHEMISTRY C

Article

pubs.acs.org/JPCC

Probing the Stress Reduction Mechanism of Diamond-Like Carbon Films by Incorporating Ti, Cr, or W Carbide-Forming Metals: Ab Initio Molecular Dynamics Simulation

Xiaowei Li, Peiling Ke, and Aiying Wang*

Key Laboratory of Marine Materials and Related Technologies, Zhejiang Key Laboratory of Marine Materials and Protective Technologies, Ningbo Institute of Materials Technology and Engineering, Chinese Academy of Sciences, Ningbo 315201, People's Republic of China

ABSTRACT: Ab initio molecular dynamics simulation based on density functional theory was performed to investigate (Ti, Cr, or W)-incorporated diamond-like carbon (DLC) films. The structure models were generated from liquid quench containing 64 atoms. The dependence of the residual compressive stress, bulk modulus and tetra-coordinated C content on the Ti, Cr, and W concentrations in the range of 1.56 to 7.81 atom % was studied. The present simulation results reveal that the residual stress strongly depends on the incorporated Ti, Cr, and W atoms. With the incorporation of Ti at 1.56 atom %, Cr at 4.69 atom %, and W at 3.13 atom % to DLC films, the compressive stress was reduced by 46.9%, 81.4%, and 82.5%, respectively, without obvious deterioration of the mechanical properties. However, at higher Ti, Cr, and W concentrations, the compressive stress increased for each case, which was consistent with the experimental results. Structural analysis using both the bond angle and bond length distributions indicates that the small amount of Ti or W incorporation efficiently relaxes both the highly distorted bond angles and bond lengths, whereas the Cr incorporation only relaxes the distorted bond lengths, which decreases the residual compressive stress and provides theoretical explanations for the experiments.

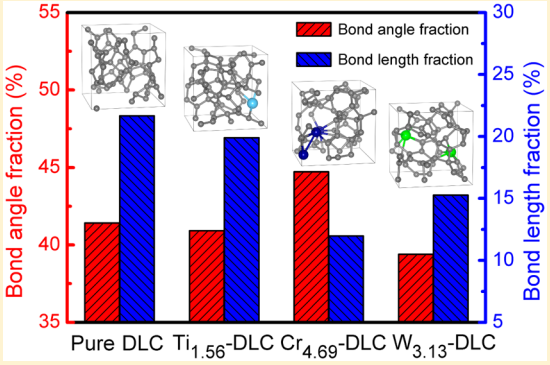

1. INTRODUCTION

Diamond-like carbon (DLC) films are widely investigated because of their unique structures and many technologically important mechanical, electronic, optical, and magnetic properties.[1] DLC films are used as a protective coating in various industrial applications and are considered in the fields of solar cell, magnetic-disk storage devices, medical application, etc.[2−6] To tailor the properties of DLC films for the desired technological applications, particularly to reduce the high level of residual compressive stress, which deteriorates the adhesion between the film and the substrate and leads to failure of the coated surface, other elements such as Ti, W, Cr, Ni, Cu, and Ag are often incorporated into the carbon matrix.[7−14] Compared with the addition of soft and ductile Ni, Cu, or Ag into amorphous carbon matrix, the alloying of DLC with the carbide-forming element (Ti, W, or Cr) can significantly decrease the stress without seriously deteriorating the hardness because hard carbide nanoparticulates form.[7−9] For example, Wang et al.[8,15] revealed that when the incorporated W atoms were dissolved in the carbon matrix without forming a WC_{1-x} phase, the pivotal action of the W atoms reduced the stain energy that appeared from the distortion of the bond angles, which significantly reduced the residual stress.

It is well-known that in metal-incorporated DLC (Me-DLC) films, the residual compressive stress is closely related to the distorted atomic bond structure. However, although the incorporation of metal atoms introduces complexity to the structure, because of the limited experimental characterization of the atomic bond structure, the effect of incorporated metal atoms on the atomic bond structure from the atomic-scale viewpoint has not been clarified, which causes the phenomenological explanation of the stress reduction mechanism. Theoretical simulation technique provides a robust method for in-depth insight into the atomic bond structure and clears the stress reduction mechanism for Me-DLC films. Until now, many simulation works have reproduced the structure and property variations of DLC films with the kinetic energy of deposited carbon atoms using the classical molecular dynamics (MD) simulation, which helps us understand the deposition process at the atomic scale.[16−18] However, most previous computational results focused on the mechanism of sp^3 bond formation and the dependence of the atomic bond structure on the kinetic energy of the deposited species in pure carbon or hydrocarbon systems. In contrast, computational study on the metal-element incorporation in Me-DLC films is highly limited, particularly for the direct simulation of the Me-DLC film growth using classical MD simulation.

Received: January 3, 2015
Revised: February 27, 2015
Published: March 2, 2015

DOI: 10.1021/acs.jpcc.5b00058
J. Phys. Chem. C 2015, 119, 6086−6093

Recently, Choi et al.[19] performed first-principles calculations on three typical metals, namely, Mo, Ag, and Al, as the transition, noble, and simple metal in the Me−C system, respectively, and provided an explanation for the stress evolution with metal addition based on the atomic bond characteristics. Li et al.[20] also revealed the bond characteristics between all transition metal (TM) atoms and the C atom using first-principles calculation with the tetrahedral-bond model, and showed that the TM−C bond characteristic with the 3*d* electrons of doped TM changed from bonding (Sc, Ti) to nonbonding (V, Cr, Mn, Fe) and finally to antibonding (Co, Ni, Cu), which accounted for the change of total energy caused by distorting the bond angles. Nevertheless, these works were highly limited to the simplified tetrahedral-bond model, which represented a special situation of the incorporated metal atoms in a carbon network. A complete atomistic understanding of the role and effect of incorporated metal atoms on the microstructure of Me-DLC films remains unable to clarify the stress reduction mechanism, and it is also indispensable for tailoring their structure and properties by guiding the deposition process.

In the present work, we performed an ab initio MD (AIMD) simulation based on density functional theory (DFT) to investigate the structural properties of various Me-DLC films. Compared with classical MD methods, which require predetermined empirical potential parameters for specified compositions, the superiority of the parameter-free AIMD method is obvious. Strong-carbide-forming metals (Ti, Cr, and W) were selected as the representative incorporated metal elements. The concentrations of Ti, Cr, and W (1.56−7.81 atom %) were selected. The residual compressive stress and bulk modulus were calculated, and the structure changes, which included both bond angles and bond lengths, were mainly analyzed. The results show that the structural evolution strongly depends on the variety and concentration of the incorporated metal atoms, which can account for the experimental changes in the physical and chemical properties of (Ti, Cr, or W)-DLC films.

2. COMPUTATIONAL DETAILS

The structural models of (Ti, Cr, or W)-DLC films were generated from liquid quench using AIMD simulation, which has been demonstrated to provide a good description of DLC materials and to reveal the intrinsic relation between the structure and properties.[21−24] The Vienna ab initio simulation package[25,26] based on DFT was used for the spin-polarized calculations with a cutoff energy of 500 eV and a generalized gradient approximation with the Perdew−Burke−Ernzerhof parametrization.[27] In this work, the initial configuration contained 64 atoms in a simple cubic supercell with constant volume and periodic boundary conditions throughout the simulation system that has been proved to be suitable and accurate to reveal the characteristics of amorphous carbon systems and save the required computation time.[23,28,29] To obtain Ti-, Cr-, and W-incorporated DLC systems, the system was first equilibrated at 8000 K for 1 ps to become completely liquid and eliminate its correlation to the initial configuration using a canonical ensemble with a Nose thermostat for temperature control. Then, the samples were cooled to 1 K within 0.5 ps, which corresponded to a cooling rate of 1.6×10^{16} K/s. Afterward, subsequent geometric optimization was performed using the conjugated gradient method,[30] where a self-consistent field was created using an energy convergence criterion of 10^{-5} eV, and a full relaxation of the atomic positions was repeated until the Hellmann−Feynman force on each atom was reduced below 0.01 eV/Å, and a gamma point only was used to sample the Brillouin zone. To check the *k*-point convergence on amorphous structure, a fully converged calculation with a grid of 4 × 4 × 4 points (64 *k* points) was performed. When only the gamma point was used, compared to a fully converged calculation with 64 *k* points, the absolute error of average binding energy of per atom was found to be accurate to better than 0.004 eV.

Five samples were obtained at the density of 2.87 g/cm^3 with various Ti, Cr, and W concentrations (1.56−7.81 atom %, which corresponded to 1, 2, 3, 4, and 5 Ti, Cr, and W atoms in the 64-atom systems). To provide more representative models of the actual Me-DLC system than the direct substitution of carbon by metal atoms in the previously generated pure DLC networks, the Ti, Cr, and W atoms were introduced by substituting carbon atoms in the liquid carbon system.[31] Pure DLC films were also involved for comparison with the Ti-, Cr-, and W-incorporated ones. Before characterizing the structure and coordination number of the Me-DLC films, the radial distribution functions (RDFs) $g(r)$ in the (Ti, Cr, or W)-DLC systems with high Ti, Cr, and W concentration (39 atom %) were first analyzed to define whether the Ti, Cr, and W atoms were bonded or nonbonded with C atoms, as shown in Figure 1. The distance to the first minimum in the RDF (inset values of Figure 1) was set as the cutoff distance R_{cut} for the C−C, Ti−Ti, C−Ti, Cr−Cr, C−Cr, W−W, and C−W bonds.[31,32] Then, the RDF, hybridization ratio, residual compressive stress, bulk modulus, and the distributions of both bond angles and bond lengths in various (Ti, Cr, or W)-DLC films were evaluated.

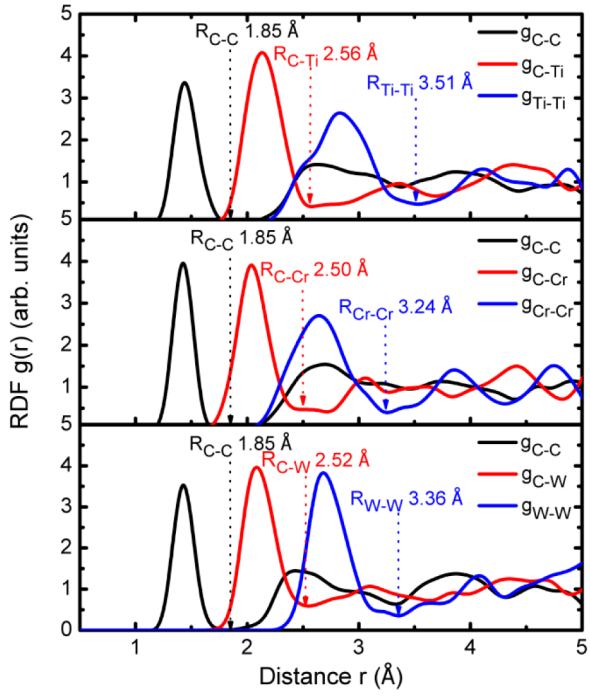

Figure 1. RDF of Ti-DLC, Cr-DLC, and W-DLC films with high Ti, Cr, and W concentrations of 39 atom %, where the inset values are the R_{cut} values for the C−C, Ti−Ti, C−Ti, Cr−Cr, C−Cr, W−W, and C−W bonds.

DOI: 10.1021/acs.jpcc.5b00058
J. Phys. Chem. C 2015, 119, 6086−6093

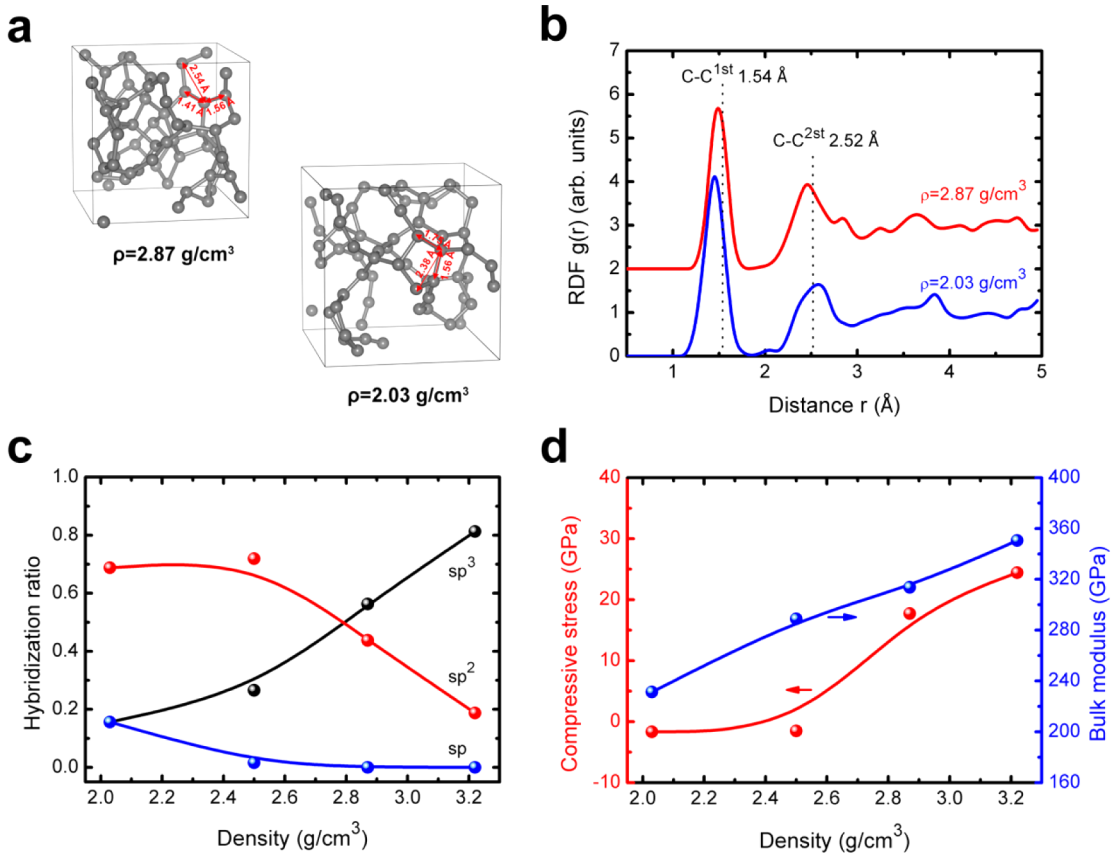

Figure 2. (a) Final morphologies and (b) RDF spectra of pure DLC films at densities of 2.87 and 2.03 g/cm^3, where the gray spheres represent the carbon atoms. (c) Hybridization ratio and (d) compressive stress and bulk modulus as a function of the densities of pure DLC films.

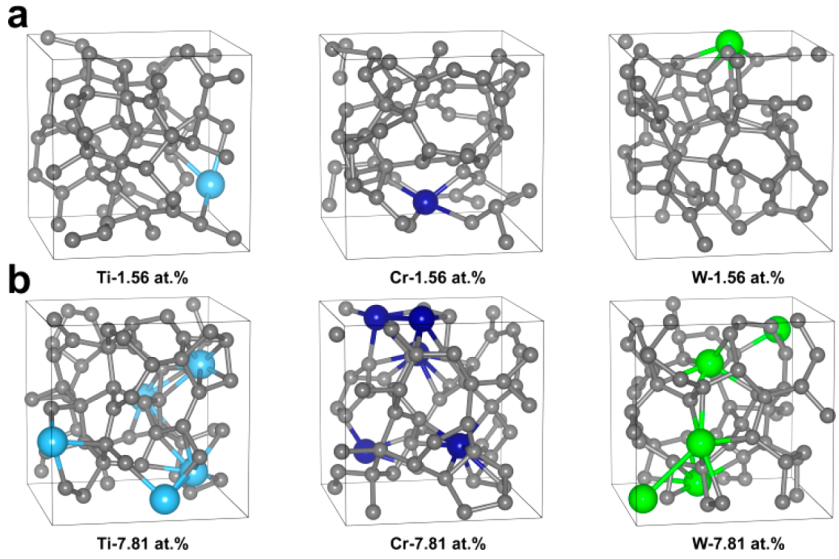

Figure 3. Final morphologies of (Ti, Cr, or W)-DLC films with the Ti, Cr, and W concentrations of (a) 1.56 and (b) 7.81 atom %, where the gray, light blue, dark blue, and green spheres represent the C, Ti, Cr, and W atoms, respectively.

3. RESULTS AND DISCUSSION

3.1. Pure DLC Films. Figure 2a shows the final morphology of a pure DLC film, which was produced at the density of 2.87 g/cm^3; for comparison, the film at the density of 2.03 g/cm^3 was also considered. It is noted that compared with the high-density (2.87 g/cm^3) film, the low-density structure of the pure DLC film (2.03 g/cm^3) is looser and contains many five-membered rings and planar chains, which are weakly cross-linked. This characteristic is typical for graphite and is not present in the sample with a higher density.

The RDF is proportional to the density of atoms at a distance r from another atom, which is a notably important parameter for the structural characterization of amorphous materials. Figure 2b presents a comparison of the RDF in pure DLC films at different densities, where the dotted lines represent the positions of the first (1.54 Å) and second nearest

DOI: 10.1021/acs.jpcc.5b00058
J. Phys. Chem. C 2015, 119, 6086−6093

neighbors (2.52 Å) of crystalline diamond. First, it is clearly observed that the RDF spectra reveal the characteristics of the amorphous structure, which are long-range disorder and short-range order. With increasing density of the pure DLC films, the first C−C nearest-neighbor peak is displaced from 1.46 Å at the density of 2.03 g/cm^3 to 1.50 Å at the density of 2.87 g/cm^3, which is related to the hybridization ratio. In addition, the first C−C nearest-neighbor peak is much smaller than that of diamond, which implies that there is high residual compressive stress.[33] The $g(r)$ value from this calculation is consistent with the previous experimental[34,35] and theoretical results,[22,23,36] which demonstrate that the simulated results reflect the nature of the actual system.

The hybridization ratio (sp^3, sp^2, and sp) and mechanical properties as functions of the densities of pure DLC films are illustrated in Figure 2c,d, where the line is a guide for view. The stress, σ, and bulk modulus, B, are computed by the equations

$$\sigma = -P = \frac{P_{xx} + P_{yy} + P_{zz}}{3} \quad (1)$$

$$B = -V\frac{dP}{dV} \quad (2)$$

$$\sigma = \frac{3}{2}P \quad (3)$$

where P is the hydrostatic pressure, P_{xx}, P_{yy}, and P_{zz} are the diagonal components of the stress tensor, V is the system volume, B is the bulk modulus; the pressure, P, is converted to the biaxial stress, σ, by multiplying the pressure by a factor of 1.5, according to the method of McKenzie (eqs 3).[37,38] The figure shows that when the density increases from 2.03 to 3.22 g/cm^3, the sp^3 content, residual compressive stress and bulk modulus gradually increase;[36] when the density is 2.87 g/cm^3, the sp^3 content and compressive stress are 56.3% and 26.6 GPa, respectively. Note that the sp content in the film is notably low and generally neglected in most DLC studies.

3.2. (Ti, Cr, or W)-Incorporated DLC Films. To display the final configurations of (Ti, Cr, or W)-DLC films with various Me concentrations, the R_{cut} values of C−Ti, Ti−Ti, C−Cr, Cr−Cr, C−W, and W−W bonds in Figure 1 were used. Figure 3a,b shows the configurations for the (Ti, Cr, or W)-DLC films with the Me concentrations of 1.56 and 7.81 atom %, respectively. After the incorporation of Ti, Cr, and W, we find that the incorporated metal atoms can bond with many C atoms around the incorporated position, whereas the low content of Ti, Cr, or W incorporation (Figure 3a) has no significant effect on the fraction of tetra-coordinated carbon atoms; there is no obvious cross-linked chains in (Ti, Cr, or W)-DLC films, as shown in Figure 3.

Figure 4 shows the RDF of (Ti, Cr, or W)-DLC films with different Ti, Cr, and W concentrations. The film for each case exhibits the typical amorphous characteristics: long-range disorder and short-range order. The first peak is known to be related to the atomic bond distance, and the second peak is related to both the bond angles and bond lengths. However, we note that with the increase in Ti, Cr, and W concentrations, the positions of the first and second nearest-neighbor peaks of the (Ti, Cr, or W)-DLC films are changed accordingly, which indicates the evolution of the atomic bond structure including bond angles and bond lengths, as will be discussed later.

The calculated residual compressive stress, bulk modulus, and tetra-coordinated C content of (Ti, Cr, or W)-DLC films

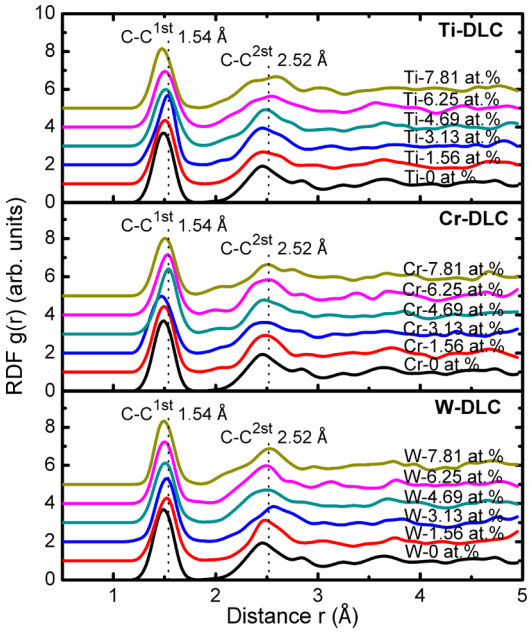

Figure 4. RDF spectra of the (Ti, Cr, or W)-DLC films with different Ti, Cr and W concentrations, where the vertical dotted lines represent the first and second nearest peak positions of crystalline diamond.

as a function of the Ti, Cr, and W concentrations are shown in Figure 5. For the Ti-DLC films in Figure 5a, the compressive stress decreases and subsequently increases with the increase in Ti concentration. When the Ti concentration in the Ti-DLC films increases from 0 to 1.56 atom %, the residual compressive stress decreases from 26.6 to 14.2 GPa; a further increase in Ti concentration to 7.81 atom % causes the compressive stress to increase to 30.6 GPa. In addition, Figure 5a shows that when the Ti concentration changes from 0 to 7.81 atom %, the bulk modulus slightly increases and subsequently decreases, which is consistent with the change in tetra-coordinated C content in Figure 5b. At a Ti concentration of 3.13 atom %, the maximal content of tetra-coordinated C reaches to 71.88%. This is attributed to the incorporated Ti atoms that could easily bond with the three-coordinated C atoms with low bonding energy. However, with further increasing Ti concentration to 7.81 atom %, many highly distorted five-coordinated C atoms with the content of 14.06% are generated, causing the decrease of tetra-coordinated C content. In general, the mechanical properties of DLC films mainly depend on the interlink matrix of tetra-coordinated C, which can account for the behavior of the bulk modulus with the Ti concentrations. By contrast, at the low Ti concentration, the compressive stress can be reduced by 46.9% without an obvious change in the mechanical properties, which is consistent with the experimental study.[7]

Figure 5c shows that when the Cr concentration in the Cr-DLC film is 4.69 atom %, the lowest compressive stress of approximately 5.0 GPa is measured, whereas further incorporation of Cr up to 7.81 atom % induces the compressive stress to increase to 16.0 GPa; the bulk modulus similarly changes with the change in tetra-coordinated C content (Figure 5b). However, the variation in the bulk modulus (max. 5.9%) is much smaller than that in the residual stress reduction (max. 81.4%). The evolution in the residual stress and mechanical properties of DLC films because of the Cr incorporation is consistent with previous work.[9,39]

DOI: 10.1021/acs.jpcc.5b00058
J. Phys. Chem. C 2015, 119, 6086−6093

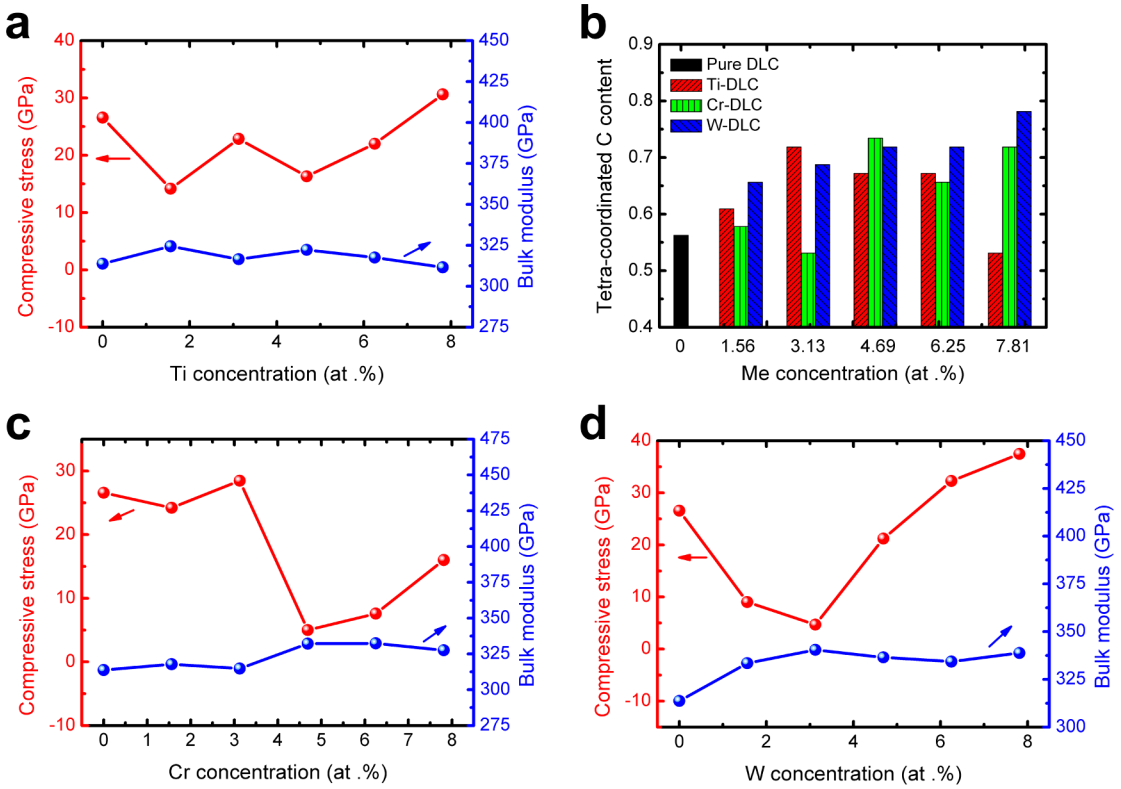

Figure 5. Compressive stress and bulk modulus of (a) Ti-DLC, (b) Cr-DLC, and (c) W-DLC films, and the (d) tetra-coordinated C content as a function of the Ti, Cr, and W concentrations.

Figure 5d shows the dependence of the compressive stress and bulk modulus on the W concentration. With the incorporation of W into DLC films, the compressive stress dramatically decreases to 4.7 GPa at W 3.13 atom %, whereas it rapidly increases to 37.5 GPa when the W concentration increases to 7.81 atom %; the bulk modulus remains almost constant at 336 ± 3 GPa for the tetra-coordinated C content in Figure 5b, which indicates that incorporating W can decrease the compressive stress by 82.5%, but the mechanical properties have no obvious deterioration, which has also been proved in Wang et al.[8,15]

For the strong-carbide-forming metals such as Ti, Cr, and W, previous works have proposed that at a low metal concentration, the dissolved metal atoms in the amorphous carbon matrix play pivotal sites, where the distorted structure can be relaxed and decrease the residual stress.[7−9] For higher metal concentrations, the metal atoms can bond with many C atoms and generate highly distorted 5-fold coordinated C atoms and the new distorted C−Ti, C−Cr, or C−W bond structure, which makes a dominant contribution to the increase in compressive stress (Figures 5). If both the residual stress and mechanical properties are closely related to the atomic bond structure of the carbon matrix, to elucidate the role of stress reduction because of various metals and various concentrations, more direct evidence for the atomic bond structure including the bond angle and length distributions must be collected.

Figures 6 through 7 show the calculated results of both bond angle and bond length distributions for Ti-DLC, Cr-DLC, and W-DLC films. For comparison, the case for pure DLC film is also considered. The black dotted lines in Figure 6 represent the stable bond angles of 120° and 109.5° for graphite and crystalline diamond, respectively; the red dotted lines in Figure 7 represent the stable bond lengths of 1.42 and 1.54 Å for graphite and diamond, respectively. For Ti-DLC films, the total bond angle distribution (Figure 6a) is mainly composed of C−C−C, C−Ti−C, and C−C−Ti bond angles (Figure 6b,c); with increasing Ti content, the peak value decreases, and the peak width shifts obviously toward the small bond angles, which are induced because of the C−Ti−C and C−C−Ti bond angles shown in Figure 6c. In Figure 7a, the total bond length distribution of Ti-DLC films mainly consists of C−C (Figure 7b) and C−Ti bond lengths, and noted that a small peak at approximately 1.85−2.5 Å is generated. Figure 7c gives the RDF spectra of Ti-DLC film with the Ti content of 7.81 atom %, which is decomposed into partial contributions from the C−C, C−Ti, and Ti−Ti. It proves that the small peak in Figure 7a originates from the C−Ti bonds because it is longer than the C−C bonds.

Li et al.[33] reported that the high compressive stress mainly originated from the distortion of both bond angles and bond lengths of the carbon network, which were below 109.5° and 1.42 Å, respectively. Thus, the C−C−C bond angles and C−C bond lengths are further focused on to gain the fractions of distorted bond angles and bond lengths, respectively. The C−C−C bond angle distribution in Ti-DLC films (Figure 6b) shows a peak at approximately 109.5°, which demonstrates the prominent contribution from the tetra-coordinated atoms for each case. The peak position with the Ti content shifts to 120°, which is related to the change in tetra-coordinated C content (Figure 5b). By integrating the C−C−C bond angle (Figure 6b) and C−C bond length distributions (Figure 7b), the fractions of distorted bond angles (<109.5°) and bond lengths (<1.42 Å) in Ti-DLC films are separately deduced, as shown in Figure 8, which clearly reveals that when the Ti content

DOI: 10.1021/acs.jpcc.5b00058
J. Phys. Chem. C 2015, 119, 6086−6093

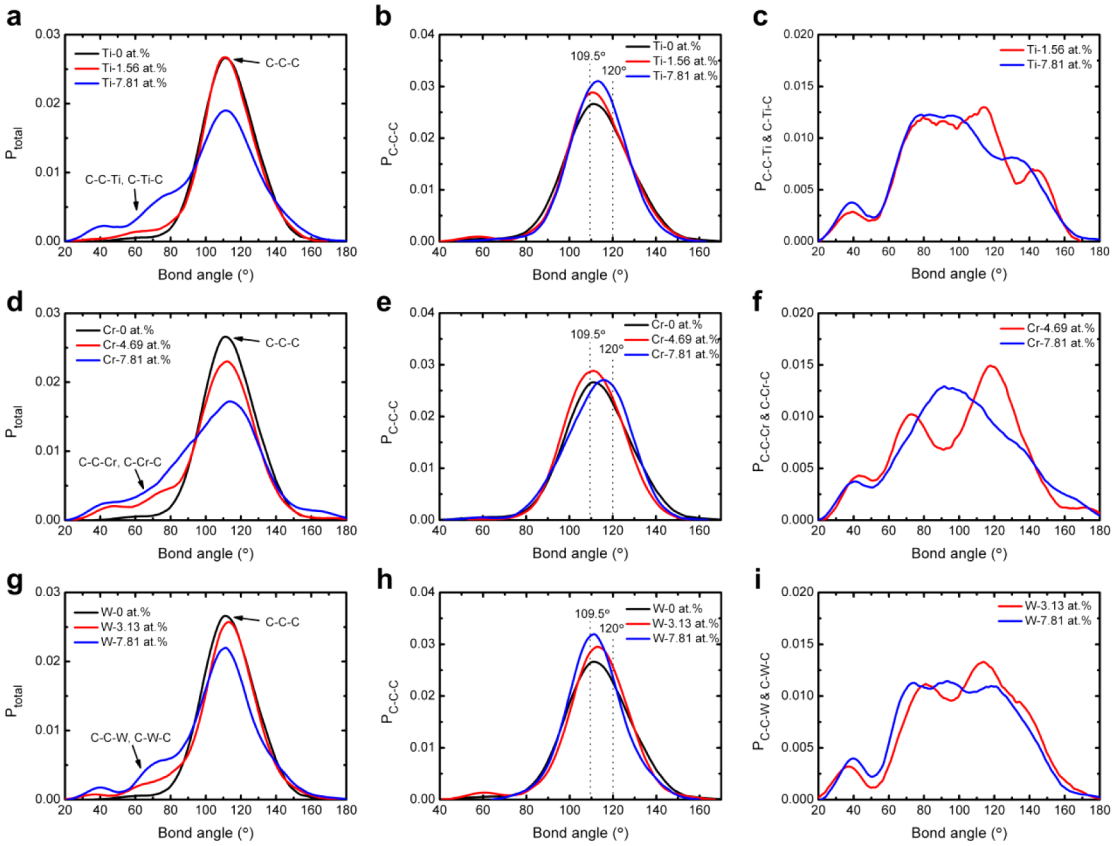

Figure 6. Bond angle distribution functions for Ti-DLC, Cr-DLC, and W-DLC films. For each case, a, d, and g are the total bond angle distributions, P_{total}, which are composed of C−C−C, C−Me−C, and C−C−Me bond angles; b, e, and h are the bond angle distributions of C−C−C, P_{C-C-C}, where the black dotted lines represent the stable bond angles of 120° and 109.5° for graphite and diamond, respectively; c, f, and i are the combined distributions of the bond angles containing Me and C atoms.

increases from 0 to 1.56 atom %, the fractions of both highly distorted bond angles (<109.5°) and bond lengths (<1.42 Å) are simultaneously reduced, which decreases the residual compressive stress of DLC films in Figure 5a. However, in the Ti-DLC film with a Ti content of 7.81 at%, the fraction of distorted bond lengths increases (Figure 7b). This can account for the increase in compressive stress.

For Cr−DLC films, the total bond angle distribution (Figure 6d) is mainly constituted by C−C−C, C−Cr−C, and C−C−Cr bond angles (Figure 6e,f); the small peak of the total bond length distribution caused by C−Cr bond changes in the range of 1.8 to 2.5 Å, as shown in Figure 7d. This is also confirmed by the C−C bond length distribution (Figure 7e) and the partial RDF spectra (Figure 7f). When the Cr content is 4.69 atom %, the fraction of distorted C−C−C bond angles increases to 44.73% from 41.42% of pure film, whereas the fraction of highly distorted C−C bond lengths significantly decreases to 11.97% from 21.67% of the pure film (Figure 8), which mainly causes the compressive-stress reduction (Figure 5c). When the Cr content increases to 7.81 atom %, the fraction of distorted C−C−C bond angles slightly decreases (Figure 6e), whereas the fraction of distorted C−C bond lengths (Figure 7e) obviously increases and contributes to the higher compressive stress of Cr-DLC films.

For W-DLC films, the similar behavior of the total bond angle distribution with W content is also observed in Figure 6g, which is from the C−C−C, C−W−C, and C−C−W bond angles (Figure 6h,i). In the total bond length distribution (Figure 7g), Figure 7h,i reveals that the small peak ranged from 1.85 to 2.5 Å is caused by the C−W bond. Figure 8 indicates that when the W content is 3.13 atom %, the fractions of both distorted bond angles and bond lengths are separately reduced to 39.40% and 15.23%, respectively, compared with the pure DLC film, which explains the significant reduction of residual compressive stress (Figure 5d). However, when the W content is 7.81 atom %, the significant increase in the fraction of distorted bond angles increases the residual compressive stress, as illustrated in Figure 6h. Therefore, these results can explain the experiments[7−9] and clarify the stress reduction mechanism caused by the Ti, Cr, and W incorporation. Furthermore, we observe that the incorporated Cr or W atoms produce a much smaller minimal stress than the Ti atoms, which is attributed to different fractions of highly distorted bond structure caused by the incorporated metal atoms.

4. CONCLUSIONS

In this study, an AIMD simulation based on DFT was successfully used to prepare (Ti, Cr, or W)-DLC films by quenching from liquid. The Ti, Cr, and W concentrations were controlled at 1.56 to 7.81 atom %. The residual compressive stress, bulk modulus and tetra-coordinated C content in each film were studied. The atomic bond structure, which includes both bond angle and bond length distributions, was mainly analyzed to clarify the stress reduction mechanism. The results show that the incorporation of a small amount of Ti, Cr, or W significantly decreases the residual compressive stress. When the Ti, Cr, and W contents were 1.56, 4.69, and 3.13 atom %, respectively, the residual compressive stress decreases to 14.2,

DOI: 10.1021/acs.jpcc.5b00058
J. Phys. Chem. C 2015, 119, 6086−6093

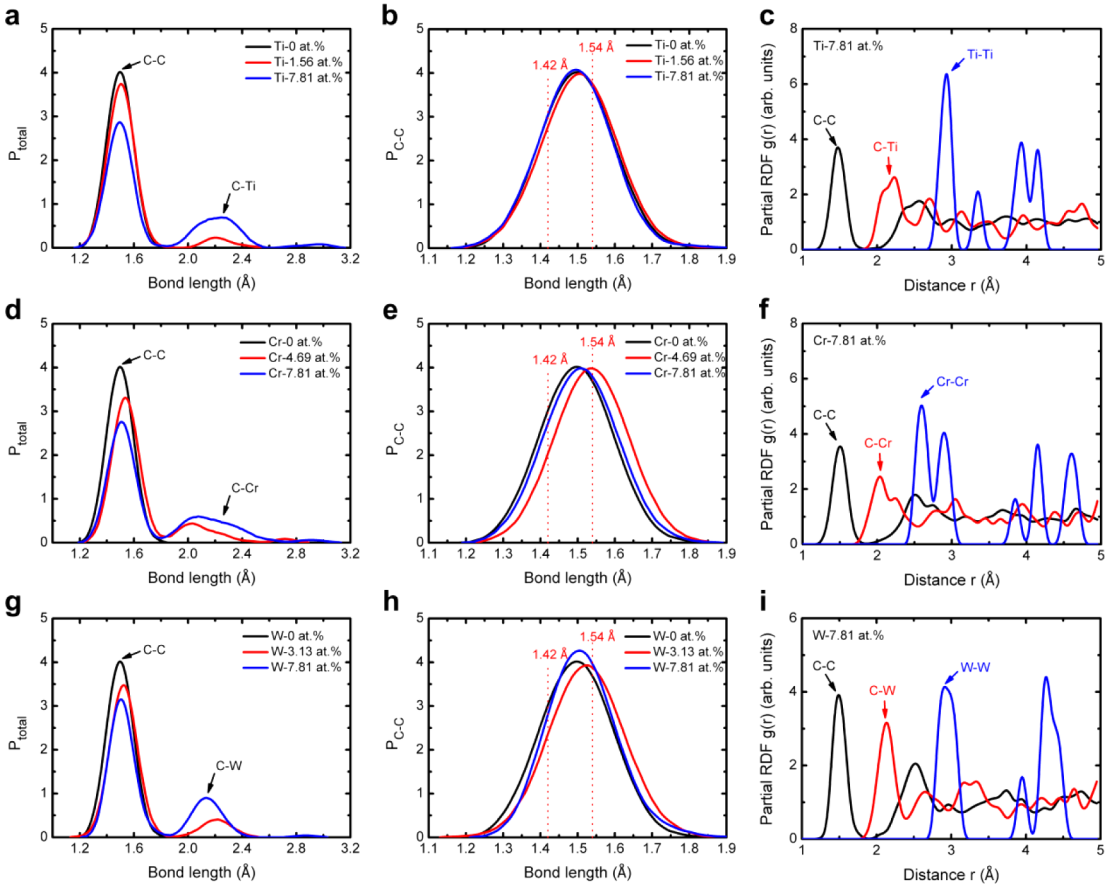

Figure 7. Bond length distribution functions for Ti-DLC, Cr-DLC, and W-DLC films. For each case, a, d, and g are the total bond length distributions, P_{total}, which are composed of C−C and C−Me bond lengths; b, e, and h are the bond length distributions of C−C, P_{C-C}, where the red dotted lines represent the stable bond lengths of 1.42 and 1.54 Å for graphite and diamond, respectively; c, f, and I are the partial RDF spectra including g_{C-C}, g_{C-Me} and g_{Me-Me} in the films with the Me content of 7.81 atom %.

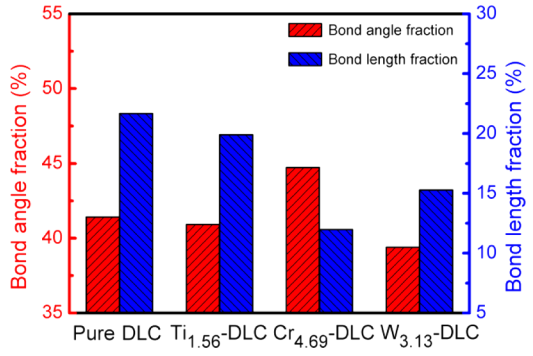

Figure 8. Fractions of distorted bond angle (<109.5°) and bond length (<1.42 Å) in pure and (Ti, Cr, or W)-DLC films. The subscripts in the horizontal axis (1.56, 4.69 and 3.13) are the concentrations of incorporated Ti, Cr, and W atoms, respectively.

5.0, and 4.7 GPa, respectively, whereas the bulk modulus had no obvious change, which was consistent with the change in the tetra-coordinated C content. By analyzing the bond angle and bond length distributions, we observed that the compressive stress reduction caused by the Ti, Cr, and W incorporation was a result of the relaxation of highly distorted bond structures, but different behaviors for the structural change were observed, where the relaxation of both distorted bond angles and bond lengths in Ti-DLC or W-DLC films resulted in the compressive stress reduction, whereas in Cr-DLC films, the incorporated Cr atoms only relaxed the distorted bond lengths. Although the current results made no comparison with the discrete organometallic molecules, which are a far cry from incorporating metal atoms in DLC films, they were consistent with previous experimental findings and provided further insight into the structure and stress reduction mechanism.

AUTHOR INFORMATION

Corresponding Author

*Tel/Fax: +86 574 86685170. E-mail: aywang@nimte.ac.cn.

Notes

The authors declare no competing financial interest.

ACKNOWLEDGMENTS

This research was financially supported by the State Key Project of Fundamental Research of China (2013CB632302, 2012CB933003), the National Natural Science Foundation of China (51402319, 51371187), and the China Postdoctoral Science Foundation (2014M551780).

REFERENCES

(1) Robertson, J. Diamond-like Amorphous Carbon. *Mater. Sci. Eng.* **2002**, *37*, 129−281.

(2) Lettington, A. H. Applications of Diamond-like Carbon Thin Films. *Carbon* **1998**, *36*, 555−560.

DOI: 10.1021/acs.jpcc.5b00058
J. Phys. Chem. C 2015, 119, 6086−6093

(3) Brand, J.; Gadow, R.; Killinger, A. Application of Diamond-like Carbon Coatings on Steel Tools in the Production of Precision Glass Components. *Surf. Coat. Technol.* **2004**, *180−181*, 213−217.
(4) Hauert, R. A Review of Modified DLC Coatings for Biological Applications. *Diamond Relat. Mater.* **2003**, *12*, 583−589.
(5) Casiraghi, C.; Robertson, J.; Ferrari, A. C. Diamond-like Carbon for Data and Beer Storage. *Mater. Today* **2007**, *10*, 44−53.
(6) Robertson, J. Requirements of Ultrathin Carbon Coatings for Magnetic Storage Technology. *Tribol. Int.* **2003**, *36*, 405−415.
(7) Dai, W.; Ke, P.; Moon, M.-W.; Lee, K.-R.; Wang, A. Investigation of the Microstructure, Mechanical Properties and Tribological Behaviors of Ti-Containing Diamond-like Carbon Films Fabricated by a Hybrid Ion Beam Method. *Thin Solid Films* **2012**, *520*, 6057−6063.
(8) Wang, A.-Y.; Lee, K.-R.; Ahn, J.-P.; Han, J. H. Structure and Mechanical Properties of W Incorporated Diamond-Like Carbon Films Prepared by a Hybrid Ion Beam Deposition Technique. *Carbon* **2006**, *44*, 1826−1832.
(9) Dai, W.; Wu, G.; Wang, A. Preparation, Characterization and Properties of Cr-Incorporated DLC Films on Magnesium Alloy. *Diamond Relat. Mater.* **2010**, *19*, 1307−1315.
(10) Kukiełka, S.; Gulbiński, W.; Pauleau, Y.; Dub, S. N.; Grob, J. J. Composition, Mechanical Properties and Friction Behavior of Nickel/Hydrogenated Amorphous Carbon Composite Films. *Surf. Coat. Technol.* **2006**, *200*, 6258−6262.
(11) Ma, K.; Yang, G.; Yu, L.; Zhang, P. Synthesis and Characterization of Nickel-Doped Diamond-Like Carbon Film Electrodeposited at a Low Voltage. *Surf. Coat. Technol.* **2010**, *204*, 2546−2550.
(12) Dwivedi, N.; Kumar, S.; Malik, H. K.; Sreekumar, C.; Dayal, S.; Rauthan, C. M. S. Investigation of Properties of Cu Containing DLC Films Produced by PECVD Process. *J. Phys. Chem. Solids* **2012**, *73*, 308−316.
(13) Choi, H. W.; Choi, J.-H.; Lee, K.-R.; Ahn, J.-P.; Oh, K. H. Structure and Mechanical Properties of Ag-Incorporated DLC Films Prepared by a Hybrid Ion Beam Deposition System. *Thin Solid Films* **2007**, *516*, 248−251.
(14) Pei, Y. T.; Chen, C. Q.; Shaha, K. P.; Hosson, J. Th. M. De.; Bradley, J. W.; Voronin, S. A.; Čada, M. Microstructural Control of TiC/a-C Nanocomposite Coatings with Pulsed Magnetron Sputtering. *Acta. Mater.* **2008**, *56*, 696−709.
(15) Wang, A.-Y.; Ahn, H.-S.; Lee, K.-R.; Ahn, J.-P. Unusual Stress Behavior in W-Incorporated Hydrogenated Amorphous Carbon Films. *Appl. Phys. Lett.* **2005**, *86*, 111902−1−3.
(16) Zheng, B.; Zheng, W. T.; Yu, S. S.; Tian, H. W.; Meng, F. L.; Wang, Y. M.; Zhu, J. Q.; Meng, S. H.; He, X. D.; Han, J. C. Growth of Tetrahedral Amorphous Carbon Film: Tight-Binding Molecular Dynamics Study. *Carbon* **2005**, *43*, 1976−1983.
(17) Neyts, E.; Bogaerts, A.; Gijbels, R.; Benedikt, J.; van de Sanden, M. C. M. Molecular Dynamics Simulation for the Growth of Diamond-like Carbon Films from Low Kinetic Energy Species. *Diamond Relat. Mater.* **2004**, *13*, 1873−1881.
(18) Pailthorpe, B. A. Molecular-Dynamics Simulations of Atomic Processes at the Low-Temperature Diamond (111) Surface. *J. Appl. Phys.* **1991**, *70*, 543−547.
(19) Choi, J.-H.; Lee, S.-C.; Lee, K.-R. A First-Principles Study on the Bond Characteristics in Carbon Containing Mo, Ag, or Al Impurity Atoms. *Carbon* **2008**, *46*, 185−188.
(20) Li, X.; Lee, K.-R.; Wang, A. Chemical Bond Structure of Metal-Incorporated Carbon System. *J. Comput. Theor. Nanos.* **2013**, *10*, 1688−1692.
(21) Bilek, M. M. M.; McKenzie, D. R.; McCulloch, D. G.; Goringe, C. M. Ab Initio Simulation of Structure in Amorphous Hydrogenated Carbon. *Phys. Rev. B* **2000**, *62*, 3071−3077.
(22) McCulloch, D. G.; McKenzie, D. R.; Goringe, C. M. Ab Initio Simulations of the Structure of Amorphous Carbon. *Phys. Rev. B* **2000**, *61*, 2349−2355.
(23) Zheng, B.; Zheng, W. T.; Zhang, K.; Wen, Q. B.; Zhu, J. Q.; Meng, S. H.; He, X. D.; Han, J. C. First-Principle Study of Nitrogen Incorporation in Amorphous Carbon. *Carbon* **2006**, *44*, 962−968.
(24) Marks, N. A.; McKenzie, D. R.; Pailthorpe, B. A.; Bernasconi, M.; Parrinello, M. Microscopic Structure of Tetrahedral Amorphous Carbon. *Phys. Rev. Lett.* **1996**, *76*, 768−771.
(25) Kresse, G.; Furthmüller, J. Efficiency of Ab Initio Total Energy Calculations for Metals and Semiconductors Using Plane-Wave Basis Set. *Comput. Mater. Sci.* **1996**, *6*, 15−50.
(26) Kresse, G.; Furthmüller, J. Efficient Iterative Schemes for Ab Initio Total-Energy Calculations Using a Plane-Wave Basis Set. *Phys. Rev. B* **1996**, *54*, 11169−11186.
(27) Perdew, J. P.; Burke, K.; Ernzerhof, M. Generalized Gradient Approximation Made Simple. *Phys. Rev. Lett.* **1996**, *77*, 3865−3868.
(28) Alvarez, F.; Díaz, C. C.; Valladares, R. M.; Valladares, A. A. Ab Initio Generation of Amorphous Carbon Structures. *Diamond Relat. Mater.* **2002**, *11*, 1015−1018.
(29) Marks, N. A.; McKenzie, D. R.; Pailthorpe, B. A.; Bernasconi, M.; Parrinello, M. Ab Initio Simulation of Tetrahedral Amorphous Carbon. *Phys. Rev. B* **1996**, *54*, 9703−9714.
(30) Gillan, M. J. Calculation of the Vacancy Formation Energy in Aluminum. *J. Phys.: Condens. Matter* **1989**, *1*, 689−711.
(31) Jornada, F. H.; Gava, V.; Martinotto, A. L.; Cassol, L. A.; Perottoni, C. A. Modeling of Amorphous Carbon Structures with Arbitrary Structural Constraints. *J. Phys.: Condens. Matter* **2010**, *22*, 395402−1−8.
(32) Haerle, R.; Galli, G.; Baldereschi, A. Structural Models of Amorphous Carbon Surfaces. *Appl. Phys. Lett.* **1999**, *75*, 1718−1720.
(33) Li, X.; Ke, P.; Zheng, H.; Wang, A. Structural Properties and Growth Evolution of Diamond-Like Carbon Films with Different Incident Energies: A Molecular Dynamics Study. *Appl. Surf. Sci.* **2013**, *273*, 670−675.
(34) Li, F.; Lannin, J. S. Radial Distribution Function of Amorphous Carbon. *Phys. Rev. Lett.* **1990**, *65*, 1905−1908.
(35) Gilkes, K. W. R.; Gaskell, P. H.; Robertson, J. Comparison of Neutron Scattering Data for Tetrahedral Amorphous Carbon with Structural Models. *Phys. Rev. B* **1995**, *51*, 12303−12312.
(36) Koivusaari, K. J.; Rantala, T. T.; Leppävuori, S. Calculated Electronic Density of States and Structural Properties of Tetrahedral Amorphous Carbon. *Diamond Relat. Mater.* **2000**, *9*, 736−740.
(37) McKenzie, D. R.; Muller, D.; Pailthorpe, B. A. Compressive Stress Induced Formation of Thin Film Tetrahedral Amorphous Carbon. *Phys. Rev. Lett.* **1991**, *67*, 773−776.
(38) Marks, N. A. Evidence for Subpicosecond Thermal Spikes in the Formation of Tetrahedral Amorphous Carbon. *Phys. Rev. B* **1997**, *56*, 2441−2446.
(39) Dai, W.; Ke, P.; Wang, A. Microstructure and Property Evolution of Cr-DLC Films with Different Cr Content Deposited by a Hybrid Beam Technique. *Vacuum* **2011**, *85*, 792−797.

DOI: 10.1021/acs.jpcc.5b00058
J. Phys. Chem. C 2015, 119, 6086−6093